SUPPORTING INFORMATION

Remarkable enhancement in ligand-exchange reactivity of thiolate-protected Au_{25} nanocluster by single Pd atom doping

Yoshiki Niihori,[†] Wataru Kurashige,[†] Miku Matsuzaki,[†] and Yuichi Negishi*[†,‡]

[†]Department of Applied Chemistry, Faculty of Science, and [‡]Research Institute for Science and Technology, Energy and Environment Photocatalyst Research Division, Tokyo University of Science, 1-3 Kagurazaka, Shinjuku-ku, Tokyo 162-8601, Japan.

I. Experiments

A. Synthesis of $[Au_{25}(SC_{12}H_{25})_{18}]^-$ and $[PdAu_{24}(SC_{12}H_{25})_{18}]^0$

$[Au_{25}(SC_{12}H_{25})_{18}]^-$ and $[PdAu_{24}(SC_{12}H_{25})_{18}]^0$ were synthesized by the methods reported in our previous studies.[1,2]

B. Ligand exchange reactions between cluster and incoming thiol

0.14 μmol of $[Au_{25}(SC_{12}H_{25})_{18}]^-$ or $[PdAu_{24}(SC_{12}H_{25})_{18}]^0$ was dissolved in 500 μL of dichloromethane. To this solution, 140 μmol of $C_nH_{2n+1}SH$ (n = 6, 8, 10, or 16) or PhC_2H_4SH was added and the solution was stirred at room temperature. At each reaction time, 5 μL of the solution was separated, washed with a mixture of methanol and water to remove excess thiols, and then characterized by matrix-assisted laser desorption ionization (MALDI) mass spectrometry.

C. Ligand exchange reaction between two kinds of clusters

0.07 μmol of $[Au_{25}(SC_{12}H_{25})_{18}]^-$ or $[PdAu_{24}(SC_{12}H_{25})_{18}]^0$ was dissolved in 250 μL of dichloromethane. To this solution, 0.07 μmol of $[Au_{25}(SC_{10}H_{21})_{18}]^-$ or $[PdAu_{24}(SC_{10}H_{21})_{18}]^0$ was added and the solution was stirred at room temperature. At each reaction time, 5 μL of the solution was separated and then characterized by MALDI mass spectrometry.

D. Characterization

MALDI mass spectra were collected using a linear time-of-flight mass spectrometer (Applied Biosystem, Voyager Linear RD VDA 500) using a nitrogen laser (wavelength: 337 nm). High-resolution MALDI mass spectra (Figures S3) were collected using a spiral time-of-flight mass spectrometer (JEOL Ltd., JMS−S3000) using a semiconductor laser (wavelength: 349 nm). In the MALDI experiments, *trans*-2-[3-(4-*tert*-butylphenyl)-2-methyl-2-propenylidene]malononitrile (DCTB) was used as the matrix. The cluster-to-matrix ratio was set to 1:1000.

Electrospray ionization (ESI) mass spectrometry was performed using a Fourier-transform mass spectrometer (Bruker, Solarix). 1 mg/mL of toluene/acetonitrile (1:1, v:v) solution of $[Au_{25}(SC_{12}H_{25})_{18}]^-$ or $[PdAu_{24}(SC_{12}H_{25})_{18}]^0$ was electrosprayed at a flow rate of 800 μL/h. In the mass analysis of $[PdAu_{24}(SC_{12}H_{25})_{18}]^0$, a small amount of $(C_4H_9)_4N^+$ was added to the solution to observe the neutral $[PdAu_{24}(SC_{12}H_{25})_{18}]^0$ as a cation.

UV–Vis absorption spectra of the clusters were recorded in toluene at ambient temperature with a spectrometer (JASCO, V-630).

II. Analysis

The average numbers of exchanged ligands, $x_{ave,}$ were estimated as

$$x_{\mathrm{ave}} = \sum_{x=0}^{18} x \frac{I(x)}{\left(\sum_{y=0}^{18} I(y) \right)} \qquad (1)$$

where x and y are the number of exchanged ligands and $I(x)$ and $I(y)$ are the ion intensities observed in the mass spectra for each x and y, respectively.

III. Characterization

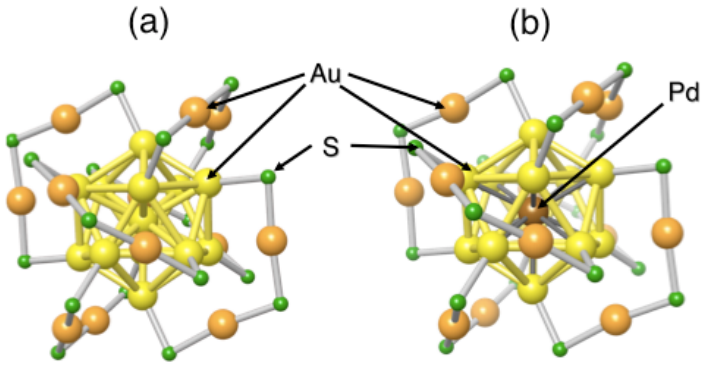

Figure S1. Structural representation of (a) $Au_{25}(SR)_{18}$ (Refs. 3 and 4) and (b) $PdAu_{24}(SR)_{18}$ (Ref. 2). (The R moieties are omitted for clarity in both figures.)

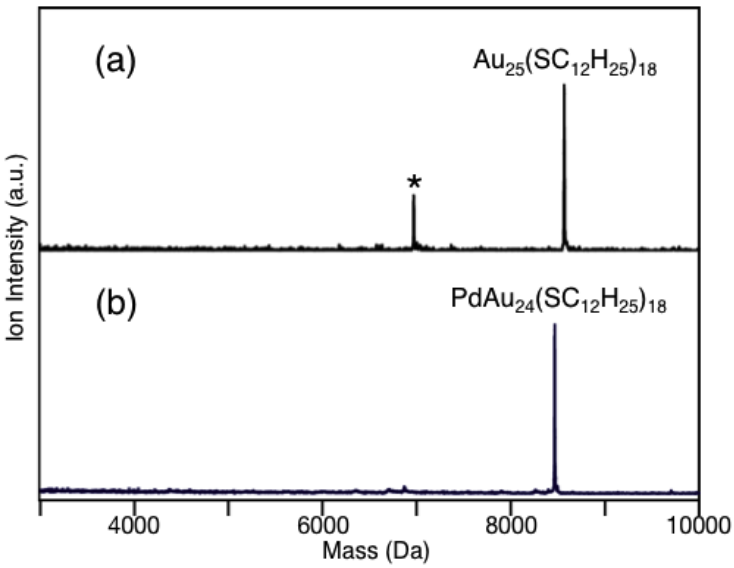

Figure S2. Negative-ion MALDI mass spectra of (a) $[Au_{25}(SC_{12}H_{25})_{18}]^-$ and (b) $[PdAu_{24}(SC_{12}H_{25})_{18}]^0$, which were used in this study. In (a), the asterisk indicates laser fragments. In (a) and (b), only peaks attributed to $[Au_{25}(SC_{12}H_{25})_{18}]^-$ and $[PdAu_{24}(SC_{12}H_{25})_{18}]^0$ were observed, indicating that $[Au_{25}(SC_{12}H_{25})_{18}]^-$ and $[PdAu_{24}(SC_{12}H_{25})_{18}]^0$ with a high purity were used in this study.

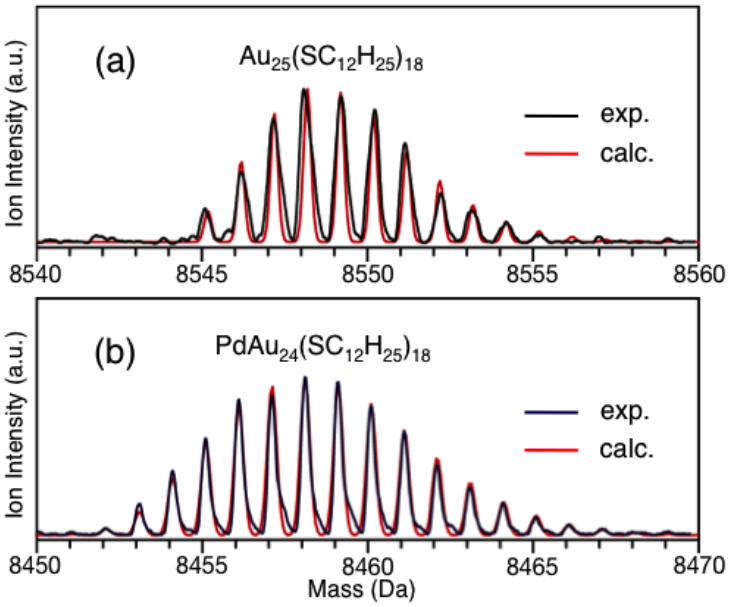

Figure S3. Comparison of experimental data obtained by high-resolution MALDI mass spectrometry with the calculated isotope pattern for (a) $[Au_{25}(SC_{12}H_{25})_{18}]^-$ and (b) $[PdAu_{24}(SC_{12}H_{25})_{18}]^0$. In (a) and (b), the experimental data is well consistent with the calculated isotope pattern, supporting the identification of the products.

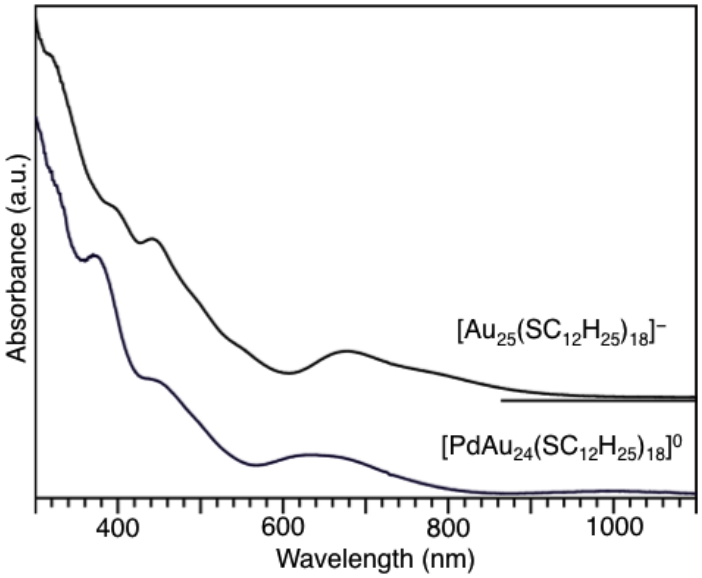

Figure S4. Optical absorption spectra of $[Au_{25}(SC_{12}H_{25})_{18}]^-$ and $[PdAu_{24}(SC_{12}H_{25})_{18}]^0$. The optical absorption spectrum of $[Au_{25}(SC_{12}H_{25})_{18}]^-$ is well consistent with that reported for anionic $[Au_{25}(SR)_{18}]^-$ (Refs. 1 and 4).

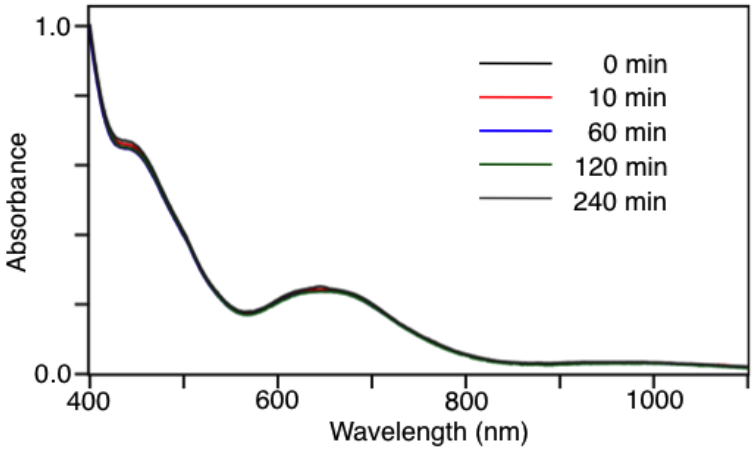

Figure S5. Time dependence of absorption spectra of a CH_2Cl_2 solution of a mixture of $[PdAu_{24}(SC_{12}H_{25})_{18}]^0$ and $C_6H_{13}SH$ (entry 7 in Table 1). Absorption spectrum exhibited only a slight change, even after 240 min. A similar phenomenon was observed for the reactions of entries 1–6 and 8–16 in Table 1.

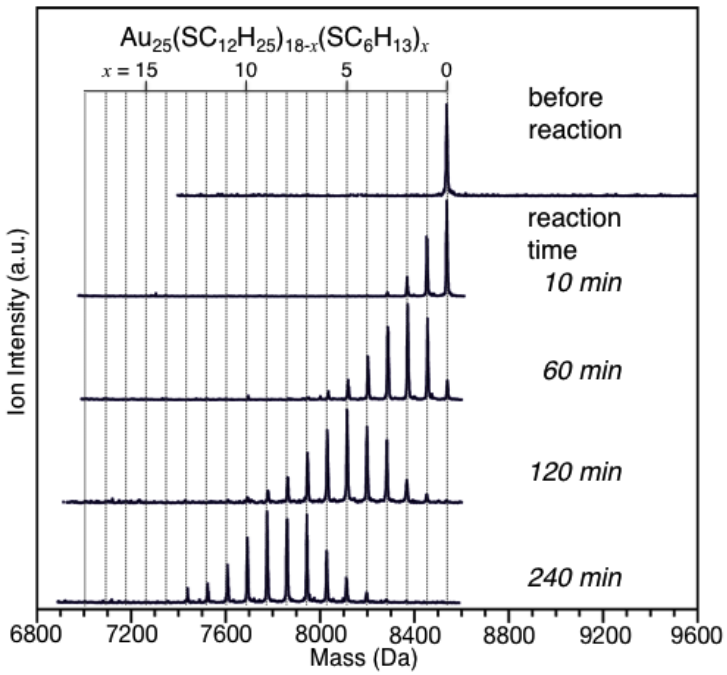

Figure S6. Negative-ion MALDI mass spectra of the product formed by the reaction between $[Au_{25}(SC_{12}H_{25})_{18}]^-$ and $C_6H_{13}SH$ in dichloromethane (entry 1 in Table 1).

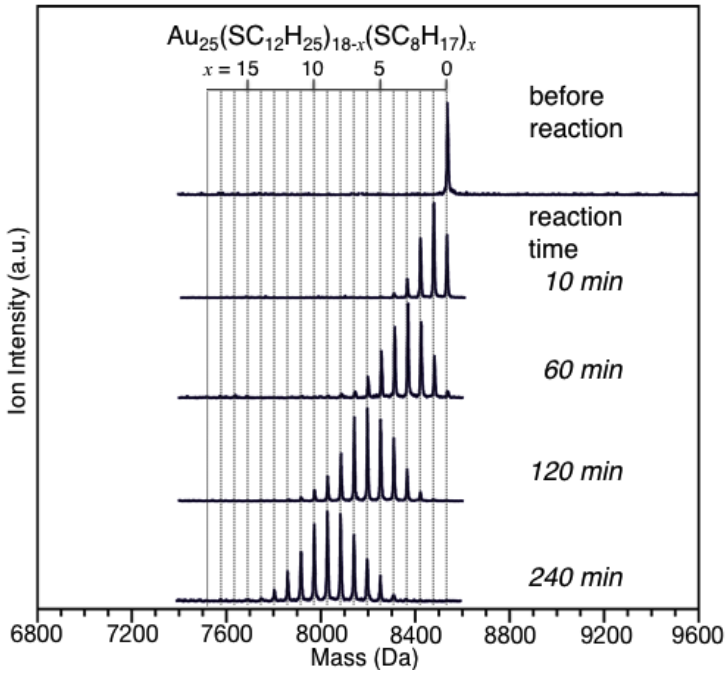

Figure S7. Negative-ion MALDI mass spectra of the product formed by the reaction between $[Au_{25}(SC_{12}H_{25})_{18}]^-$ and $C_8H_{17}SH$ in dichloromethane (entry 2 in Table 1).

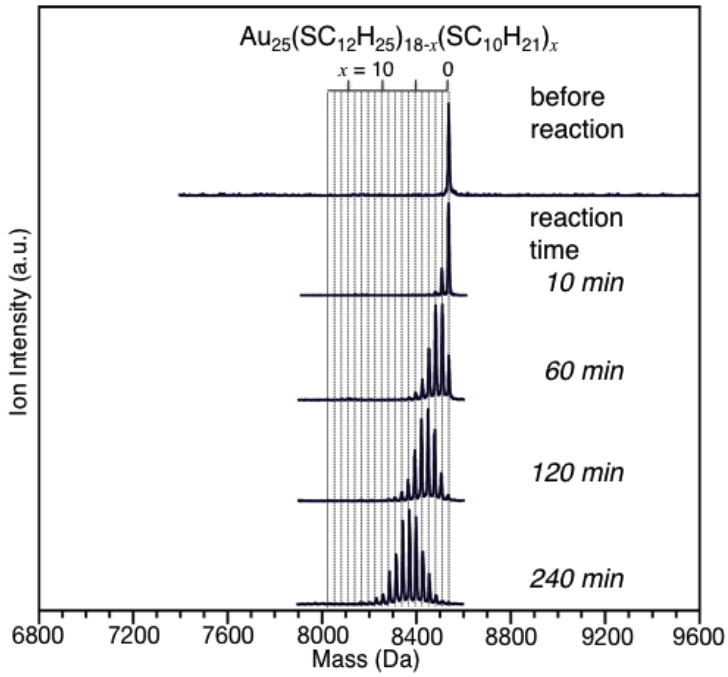

Figure S8. Negative-ion MALDI mass spectra of the product formed by the reaction between $[Au_{25}(SC_{12}H_{25})_{18}]^-$ and $C_{10}H_{21}SH$ in dichloromethane (entry 3 in Table 1).

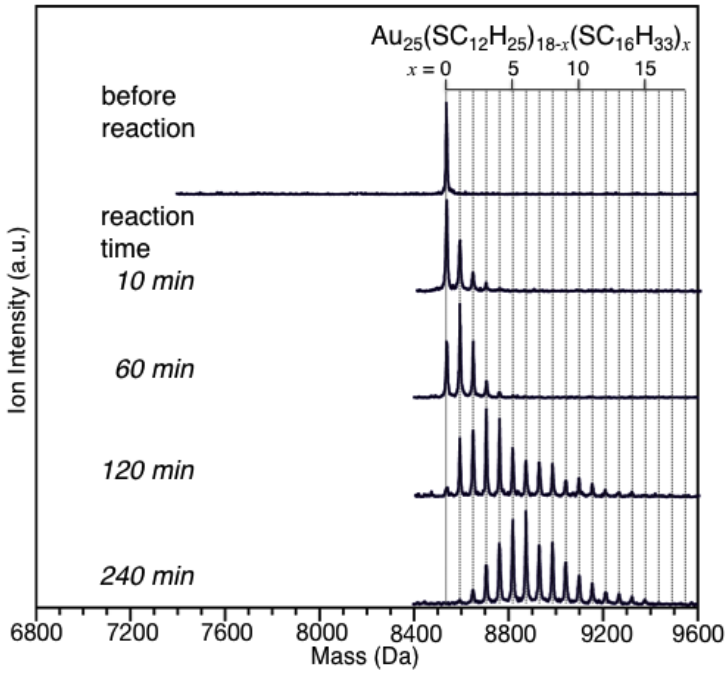

Figure S9. Negative-ion MALDI mass spectra of the product formed by the reaction between $[Au_{25}(SC_{12}H_{25})_{18}]^-$ and $C_{16}H_{33}SH$ in dichloromethane (entry 4 in Table 1).

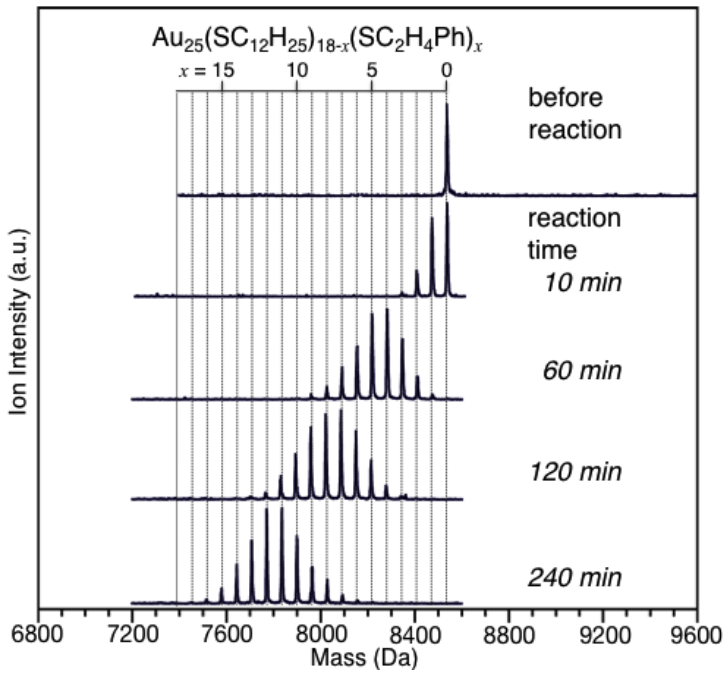

Figure S10. Negative-ion MALDI mass spectra of the product formed by the reaction between $[Au_{25}(SC_{12}H_{25})_{18}]^-$ and PhC_2H_4SH in dichloromethane (entry 5 in Table 1).

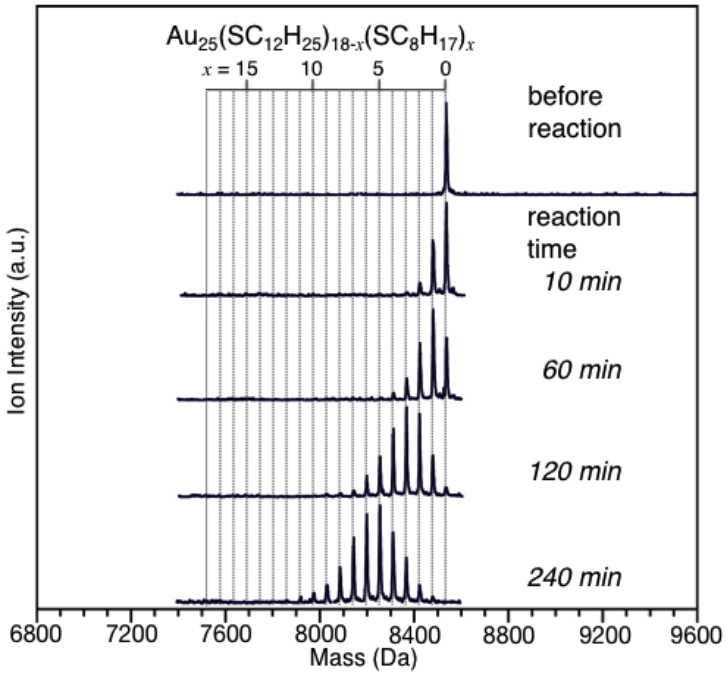

Figure S11. Negative-ion MALDI mass spectra of the product formed by the reaction between $[Au_{25}(SC_{12}H_{25})_{18}]^-$ and $C_8H_{17}SH$ in toluene (entry 6 in Table 1).

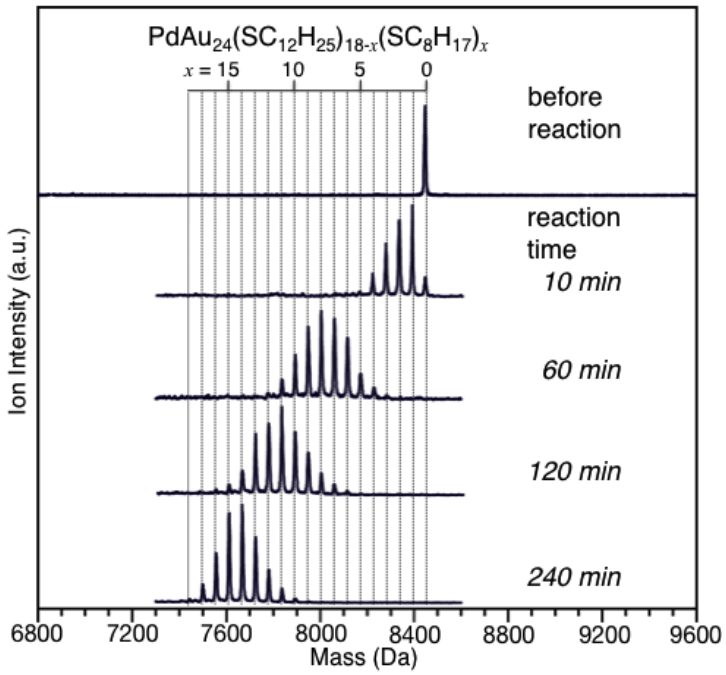

Figure S12. Negative-ion MALDI mass spectra of the product formed by the reaction between $[PdAu_{24}(SC_{12}H_{25})_{18}]^0$ and $C_8H_{17}SH$ in dichloromethane (entry 8 in Table 1).

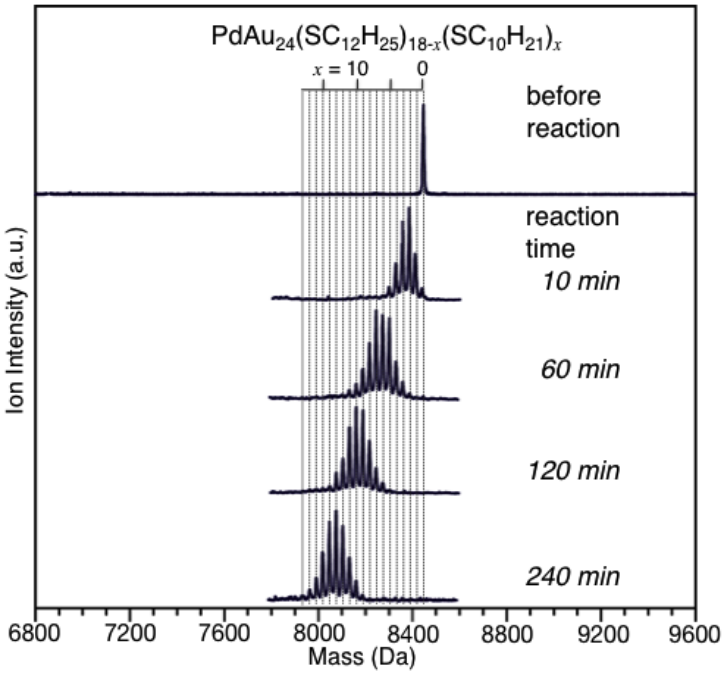

Figure S13. Negative-ion MALDI mass spectra of the product formed by the reaction between $[PdAu_{24}(SC_{12}H_{25})_{18}]^0$ and $C_{10}H_{21}SH$ in dichloromethane (entry 9 in Table 1).

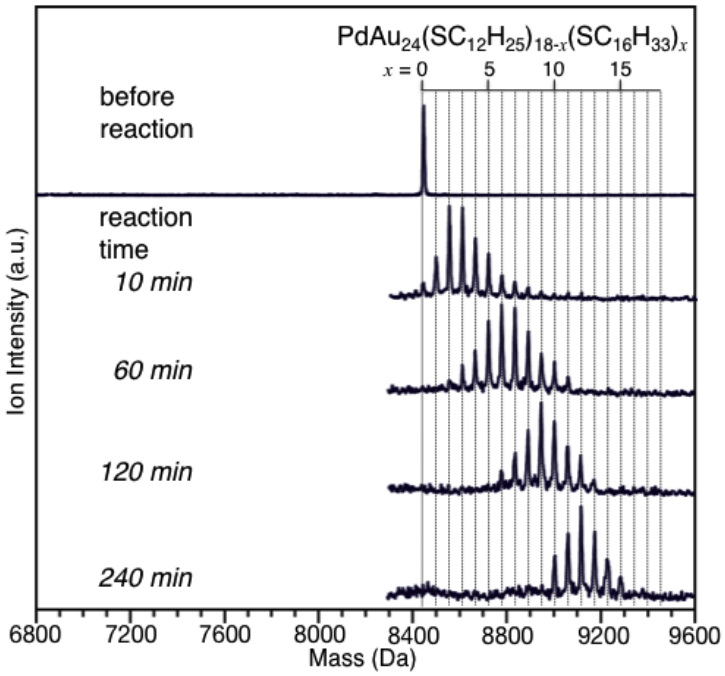

Figure S14. Negative-ion MALDI mass spectra of the product formed by the reaction between $[PdAu_{24}(SC_{12}H_{25})_{18}]^0$ and $C_{16}H_{33}SH$ in dichloromethane (entry 10 in Table 1).

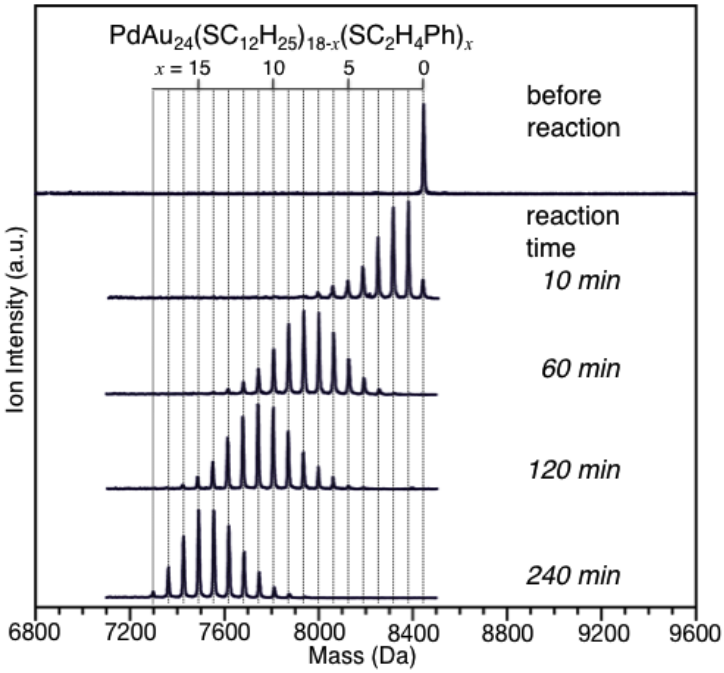

Figure S15. Negative-ion MALDI mass spectra of the product formed by the reaction between $[PdAu_{24}(SC_{12}H_{25})_{18}]^0$ and PhC_2H_4SH in dichloromethane (entry 11 in Table 1).

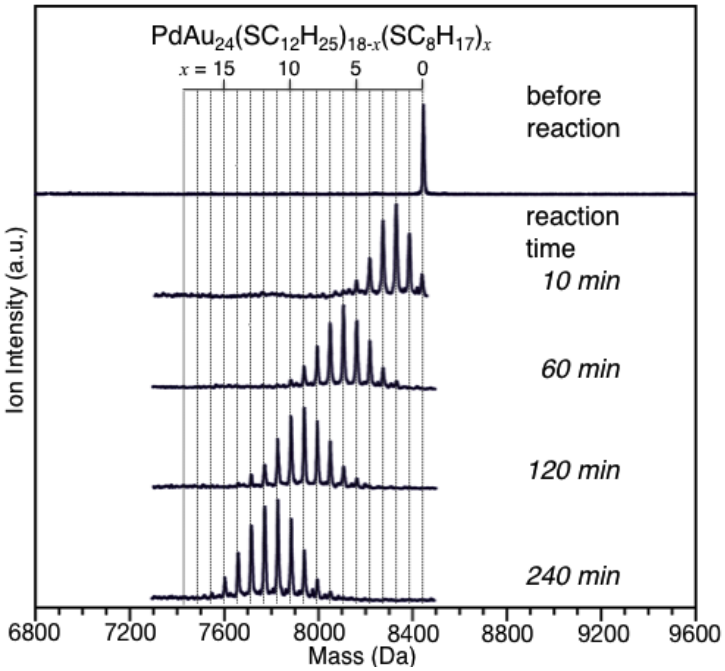

Figure S16. Negative-ion MALDI mass spectra of the product formed by the reaction between $[PdAu_{24}(SC_{12}H_{25})_{18}]^0$ and $C_8H_{17}SH$ in toluene (entry 12 in Table 1).

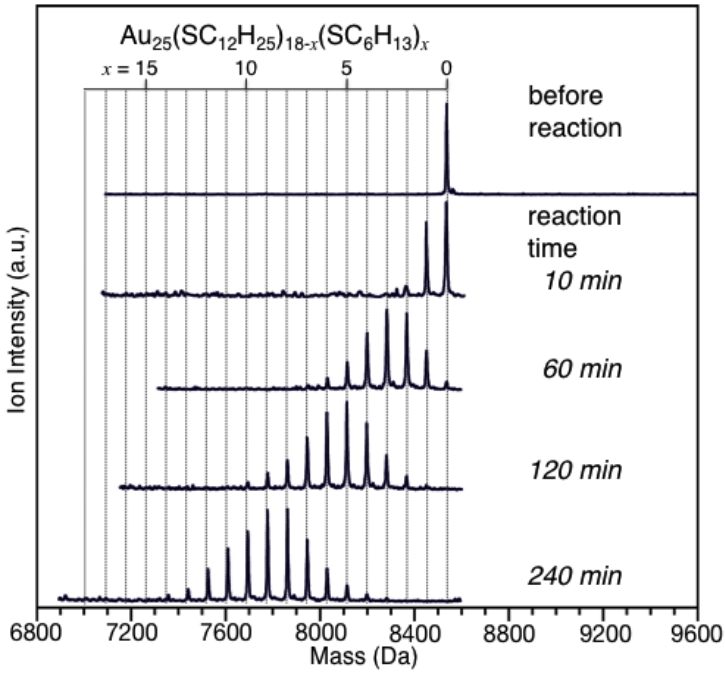

Figure S17. Negative-ion MALDI mass spectra of the product formed by the reaction between $[Au_{25}(SC_{12}H_{25})_{18}]^0$ and $C_6H_{13}SH$ in dichloromethane (entry 13 in Table 1).

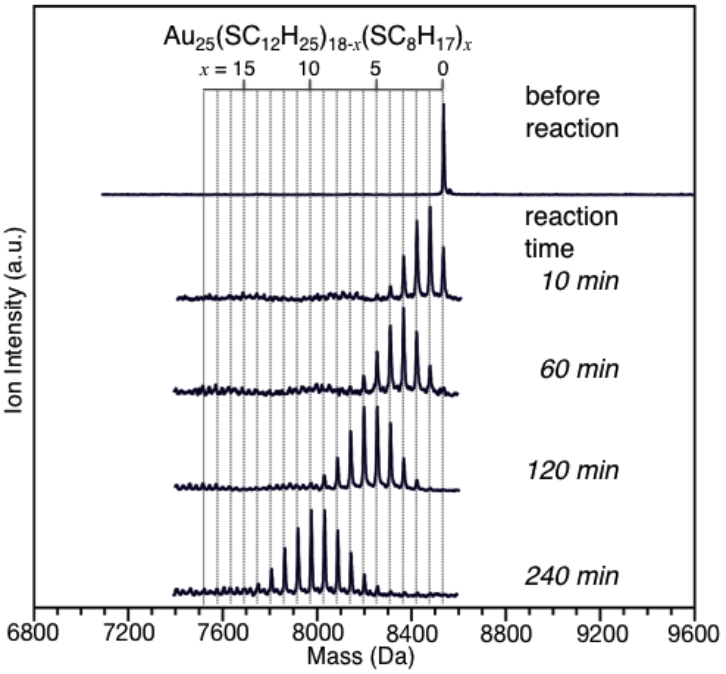

Figure S18. Negative-ion MALDI mass spectra of the product formed by the reaction between $[Au_{25}(SC_{12}H_{25})_{18}]^0$ and $C_8H_{17}SH$ in dichloromethane (entry 14 in Table 1).

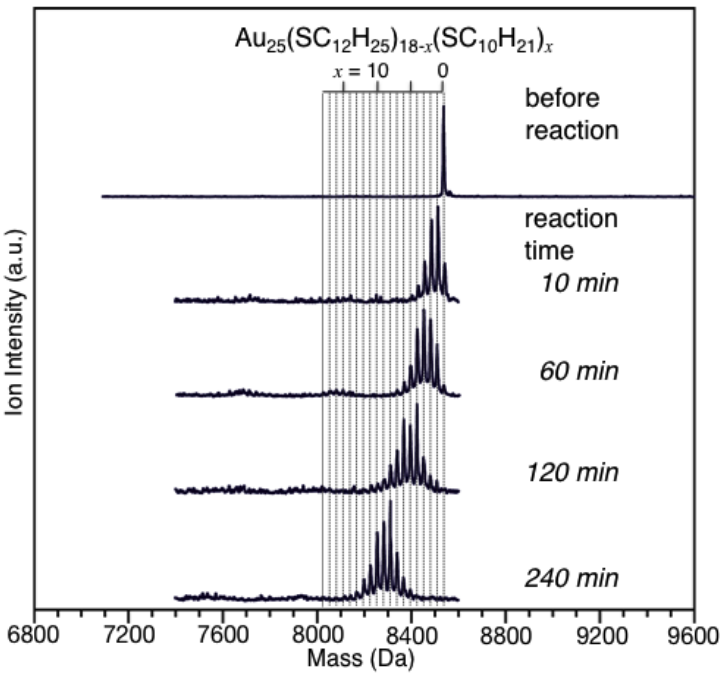

Figure S19. Negative-ion MALDI mass spectra of the product formed by the reaction between $[Au_{25}(SC_{12}H_{25})_{18}]^0$ and $C_{10}H_{21}SH$ in dichloromethane (entry 15 in Table 1).

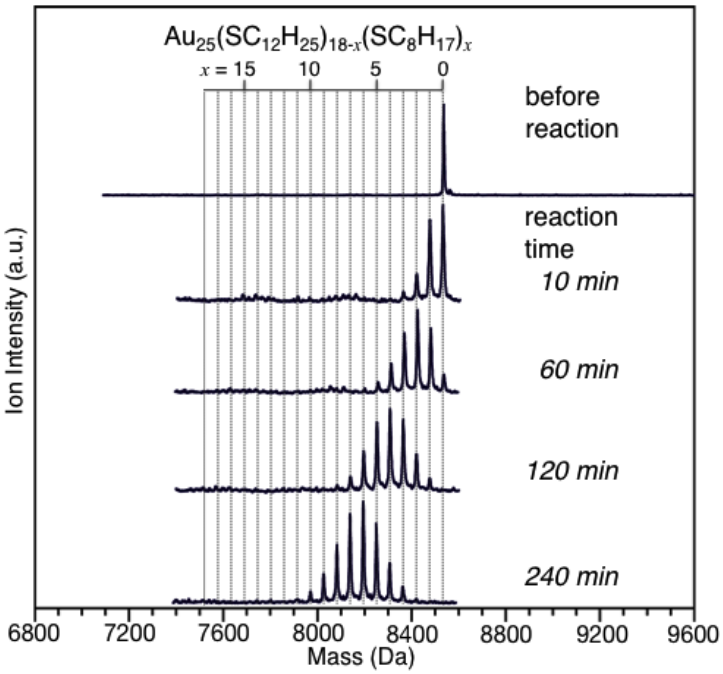

Figure S20. Negative-ion MALDI mass spectra of the product formed by the reaction between $[Au_{25}(SC_{12}H_{25})_{18}]^0$ and $C_8H_{17}SH$ in toluene (entry 16 in Table 1).

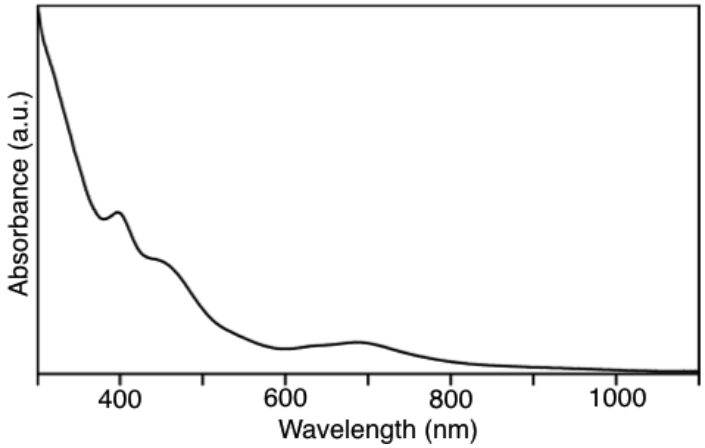

Figure S21. Optical absorption spectrum of $[Au_{25}(SC_{12}H_{25})_{18}]^0$, which was formed by leaving $[Au_{25}(SC_{12}H_{25})_{18}]^-$ in acetone for 3 days. This optical absorption spectrum is well consistent with that reported for $[Au_{25}(SC_2H_4Ph)_{18}]^0$ by Jin's group (Ref. 5).

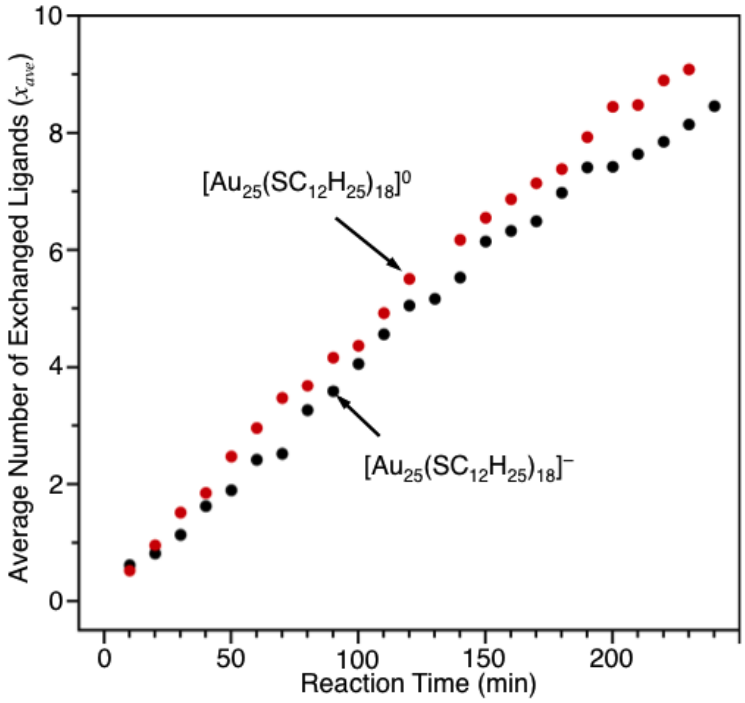

Figure S22. Plot of average number of exchanged ligands, x_{ave}, against reaction time for (red) the reaction between $[Au_{25}(SC_{12}H_{25})_{18}]^0$ and $C_6H_{13}SH$ in CH_2Cl_2 (entry 13) and (black) that between $[Au_{25}(SC_{12}H_{25})_{18}]^-$ and $C_6H_{13}SH$ in CH_2Cl_2 (entry 1). This result indicates that the reaction rate depends on the charge state of $Au_{25}(SC_{12}H_{25})_{18}$; $[Au_{25}(SC_{12}H_{25})_{18}]^0$ reacts with $C_6H_{13}SH$ faster than $[Au_{25}(SC_{12}H_{25})_{18}]^0$. A similar phenomenon was observed under the other experimental conditions (Table 1).

References

2. Negishi, Y.; Chaki, N. K.; Shichibu, Y.; Whetten, R. L.; Tsukuda, T. *J. Am. Chem. Soc.* **2007**, *129*, 11322.
3. Negishi, Y.; Kurashige, W.; Niihori, Y.; Iwasa, T.; Nobusada, K. *Phys. Chem. Chem. Phys.* **2010**, *12*, 6219.
4. Heaven, M. W.; Dass, A.; White, P. S.; Holt, K. M.; Murray, R. W. *J. Am. Chem. Soc.* **2008**, *130*, 3754.
5. Zhu, M.; Aikens, C. M.; Hollander, F. J.; Schatz, G. C.; Jin, R. *J. Am. Chem. Soc.* **2008**, *130*, 5883.
6. Zhu, M.; Eckenhoff, W. T.; Pintauer, T.; Jin, R. *J. Phys. Chem. C* **2008**, *112*, 14221.